

Potential field continuation in spatial domain: A new kernel function and its numerical scheme

Zhikui Guo, Chunhui Tao*

Key Laboratory of Submarine Geosciences, SOA, Second Institute of Oceanography, MNR, Hangzhou, 310012, China



ARTICLE INFO

Keywords:

Potential field
Downward continuation
Spatial domain
Fredholm integration
New kernel function
Surface to surface

ABSTRACT

As a significant data processing method, the potential field continuation is usually implemented in frequency domain, but rarely in spatial domain. However, the space-domain method has the advantages of being more accurate and flexible. In this study, we propose a new numerical integral approach to solve the integration equation. The algorithm can be applied to upward continuation as well as stable downward continuation, and can be used to obtain continued potential field data from a plane upward to a surface and from a surface downward to a plane. A smooth fitting curve is proposed to determine optimal iterative number for the iteration procedure of the algorithm. Both synthetic and field data are used to test the proposed approach and compare with previous studies. The numerical experiment results indicate the proposed method has a stable numerical performance and a wide range of application.

1. Introduction

Downward continuation from one observation surface to another is frequently applied to process and interpret potential field data. It results in maximizing the resolution of the continued field that are close to the source fields as well as enhance the weak signals. For instance, Li et al. (2012) applied an algorithm of stable downward continuation to enhance the magnetic data for UXO (unexploded ordnance) detection. The algorithm is also required by other data processing methods (Fedi et al., 2005; Gonçalves et al., 2017), such as frequency-domain processing (Mauri et al., 2011), edge detection (Ma and Li, 2012; Oliveira et al., 2017), map compilation consistency, as well as for the correct representation of these methods (Pilkington and Boulanger, 2017). In addition, airborne surveys (e.g. Abtahi et al., 2016) on the continent and near-seafloor surveys (e.g. Caratori et al., 2012) in the ocean are all conducted on irregular surfaces rather a horizontal plane. The observation field data could be distorted by terrain, even though filtering and correlation method can be used to eliminate this effect (e.g. Yáñez et al., 2018), potential field continuation is a much more straightforward approach, especially the spatial-domain method.

Pilkington and Boulanger (2017) discussed and compared nine different continuation methods, and classified them into two broad categories: field-based and source-based. In contrast to the source-based methods, the former involve direct approaches without the calculation

of intermediate physical quantities, and are independent of data types. Among the five field-based methods, Pilkington and Boulanger (2017) noted that downward continuation is possible for methods proposed by Xu et al. (2003) and Ivan (1986). Taylor's expression method (Blakely, 1996, pp. 323) can only deal with downward continuation from a horizontal plane to an undulant surface. To solve problem of continuation from an undulant surface to a horizontal plane, Pilkington and Thurston (2001) improved Taylor's method by assuming that the observations are located on a horizontal plane and the surface is replaced by an inverse topography (Pilkington and Boulanger, 2017). The methods by Guspí (1987) and Strakhov and Devitsyn (1965) can continue a field from surface to a plane. The former method was based on Taylor's series, while the latter one viewed downward continuation as an inverse problem that relies on the solution of a forward problem given by the well-known formula for upward continuation, followed by a simple iteration scheme to solve the problem. In all these methods, the observed field was considered as the initial guess. For the numerical algorithm strategy, iteration and regularization are the most common methods (e.g. Zhang et al., 2016; Pašteka et al., 2012; Zeng et al., 2013). Potential field continuation can also be classified into another category by numerical scheme: frequency-domain and space-domain. The former is based on the Fast Fourier Transform (FFT) which is addressed in several previous studies (e.g. Fedi and Florio, 2002; Trompat et al., 2003; Cooper, 2004; Pilkington and Boulanger, 2017). The frequency-domain

* Corresponding author.

E-mail address: taochunhuimail@163.com (C. Tao).

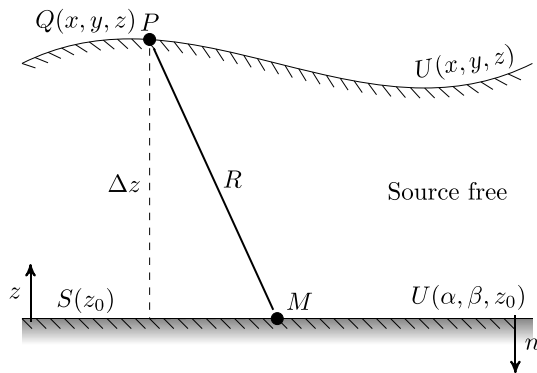


Fig. 1. Geometry for upward continuation from a horizontal plane to an arbitrary surface. Observations are made on surface S and upward continued to surface Q . Δz represents upward continued height for observation point P .

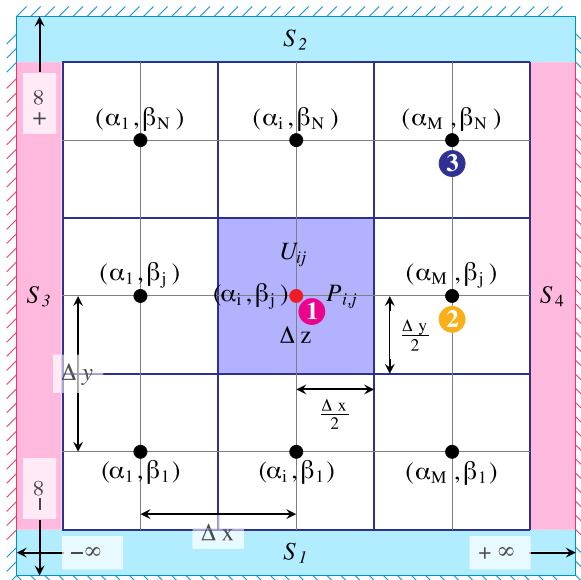


Fig. 2. Schematic diagram of integral and discretization schemes. Black solid circles are observed points on plane S . M and N represent numbers of data points in directions x and y , respectively. Blue rectangle in the center shows an integral cell for equation (4). U_{ij} and (α_i, β_j) are field and coordinates of the central point (red circle) of the integral cell, respectively. Δz is the vertical distance to the continued point P . $S_i (i = 1, 2, 3, 4)$ at the boundary represent four infinite integral regions outside the observational field region, and the three colored i ($i = 1, 2, 3$) represent horizontal positions of three continued points (see Fig. 12 and section 5). (For interpretation of the references to color in this figure legend, the reader is referred to the Web version of this article.)

methods cannot be used directly to deal with the field data on an undulate surface, e.g. downward continuation from surface to plane. Because of the nature of FFT, the data must be preprocessed before transformation, for example removal trend from the data and padding data to 2^N points, and additional problems will appear in the pre-processing procedure (Cooper, 2004). In spatial domain, however, potential field continuation can be solved directly. The upward continuation is equivalent to a matrix multiplication problem $\mathbf{K}\mathbf{U}_0 = \mathbf{U}$, where \mathbf{U}_0 is column vector of the observation field and \mathbf{K} is the kernel matrix. In contrast, the downward continuation is equivalent to an optimization problem based on the upward continuation, where \mathbf{U} is column vector of the observation field and \mathbf{U}_0 is the column vector of unknowns. The linear equations can be solved using iterative method which is widely applied in the inverse and ill-posed problems (Hansen, 2002).

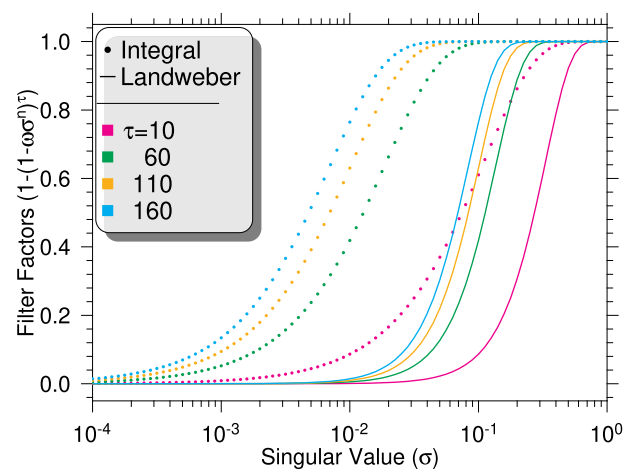


Fig. 3. The filter factor function of Integral-iteration method (dotted lines: $n = 1$) and Landweber iteration method (solid lines: $n = 2$) with different iterative numbers shown in different colors. The coefficient (ω) of each line is 0.9. (For interpretation of the references to color in this figure legend, the reader is referred to the Web version of this article.)

In case of downward continuation as an inverse problem (e.g. Liu et al., 2015; Gross et al., 2015; Wang et al., 2015) in spatial domain, its solution relies strongly on upward continuation (forward problem). Some previously reported approaches implemented a simple scheme of discretizing the kernel function to calculate the kernel matrix \mathbf{K} (e.g. Zhang et al., 2016). It should be noted that the kernel function is invalid when continuing distance is less than the minimum grid spacing of a grid data. Therefore, herein, we propose a new kernel function and a new numerical scheme for potential field data continuation from surface to horizontal plane. The new kernel function has no limitation on the continuation distance, and the new method can be used to deal with continuation from undulant surface to another arbitrary surface, not always horizontal plane. Based on the new kernel function, we developed computer program named conti2d to calculate potential field continuation in spatial domain. The program is developed in C++, using OpenMP for parallel computation and using Gmsh (Geuzaine and Jean-François, 2009) for graphical user interface (GUI). Both synthetic data and field data are used to test the numerical performance and accuracy of the method.

2. Theory

Downward continuation of potential field data from an arbitrary surface to a horizontal plane is regarded as an inverse problem, which is based on upward continuation. Herein, prior to elucidating the solution to this inverse problem in detail, we outline the mathematical background on the forward problem. The classic upward continuation formula from Blakely (1996, pp. 316), can be rewritten as,

$$U(x, y, z) = \frac{\Delta z(x, y)}{2\pi} \int_{-\infty}^{+\infty} \int_{-\infty}^{+\infty} \frac{U(\alpha, \beta, z_0)}{R^3} d\alpha d\beta \quad (1)$$

where $U(\alpha, \beta, z_0)$ is the observed field on a horizontal plane S , and $U(x, y, z)$ is the upward continued field on an irregular surface Q . Therefore, $\Delta z = z(x, y) - z_0 \geq 0$ is a function of (x, y) rather than a constant value as determined via integration (Blakely, 1996, Eq. (12.4)). Therein, $R = [(x - \alpha)^2 + (y - \beta)^2 + \Delta z^2]^{1/2}$ is the distance between any upward continued point P on surface Q and any observed point M on horizontal plane S . We specify that the z axis is directed upward and the space between Q and S is source free (Fig. 1).

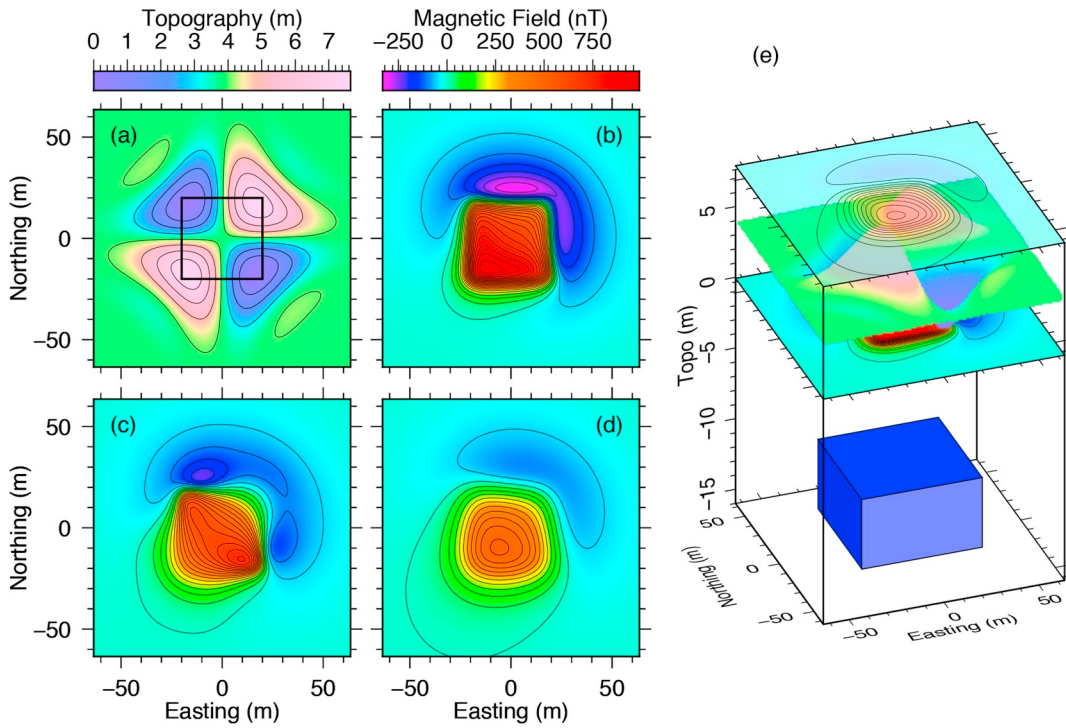


Fig. 4. Synthetic data. (a) The simulated topography which is calculated from equation (9) with $f_0 = 10$. The black rectangle represents the position of the prism. Theoretical magnetic field are computed at the plane of $z = 0$ m (b), at the plane of $z = 8$ m (d), and at a simulated topography surface (c), respectively. (e) 3-D view of model, topography and field data.

Table 1

Computation time, root mean-square error (RMSE) and relative error (RE) for continuation results in Figs. 5–8. UWC indicates upward continuation and DWC indicates downward continuation. Space and frequency representing continuation are processed in spatial domain and frequency domain, respectively. The last row is the iteration number of downward continuation.

	UWC (level→level)		DWC (level→surface)	
	space	FFT	space	space
Time (sec)	0.36	0.07	2.2	7.9
RMSE (nT)	2.13	3.40	1.76	2.4
RE (%)	1.75	2.8	1.06	1.07
Iteration	–	–	–	100
				100

2.1. Upward continuation and discretization

For equation (1), if field $U(\alpha, \beta, z_0)$ on the given plane S , apart from the source-based methods, there are two ways to solve the field $U(x, y, z)$ on surface Q . One is the FFT method (Baranov, 1975), which, however, can only process continuation plane to plane. The second is the space-domain method (e.g. Zhang et al., 2016, eq. (21)). Herein, we propose a new kernel function for the space-domain scheme. Equation (1) can be reduced into two entities with a finite integration (equation (2)), as the number and the area of the observational data are generally limited.

$$U(x, y, z) = \frac{\Delta z(x, y)}{2\pi} \int_{\alpha_1}^{\alpha_2} \int_{\beta_1}^{\beta_2} \frac{U(\alpha, \beta, z_0)}{R^3} d\alpha d\beta + \sum_{i=1}^4 O(S_i) \quad (2)$$

$$\approx \frac{\Delta z(x, y)}{2\pi} \int_{\alpha_1}^{\alpha_2} \int_{\beta_1}^{\beta_2} \frac{U(\alpha, \beta, z_0)}{R^3} d\alpha d\beta$$

where $[\alpha_1, \alpha_2]$, and $[\beta_1, \beta_2]$ represent the dimensions of observational

data in directions α and β , respectively. $O(S_i)$ ($i = 1, 2, 3, 4$) is the integration for the outside infinite regions that are shown in Fig. 2. The error due to this approximation depends on the ratio of data dimension and continuation height.

To directly solve the upward continuation in spatial domain, equation (2) is reduced to the sum of piecewise integrals (equation (3)) and discretized by the midpoint quadrature rule (Fig. 2) as

$$U_{m,n} = \frac{1}{2\pi} \sum_{i=1}^M \sum_{j=1}^N P_{m,n;i,j} U_{i,j} \quad (3)$$

Here, $U_{mn} = U(x_m, y_n, z)$ is the continued field which is discretized into similar grid of observational field $U_{ij} = U(\alpha_i, \beta_j, z_0)$. The U_{ij} is assumed as a constant in subdomain of integration (blue translucent rectangle in Fig. 2). The error due to this assumption (or approximation) depends on the resolution of the observational field data. The piecewise integral $P_{m,n;i,j}$ can be written as equation (4),

$$P_{m,n;i,j} = \Delta z \left(x_m, y_n \right) \int_{\alpha_i - \Delta x/2}^{\alpha_i + \Delta x/2} \int_{\beta_j - \Delta y/2}^{\beta_j + \Delta y/2} \frac{d\alpha d\beta}{R^3} \\ = \arctan \left(\frac{(\alpha - x_m)(\beta - y_n)}{\Delta z \left(x_m, y_n \right) \sqrt{(\alpha - x_m)^2 + (\beta - y_n)^2 + \Delta z \left(x_m, y_n \right)^2}} \right) \Big|_{\alpha_i - \Delta x/2}^{\alpha_i + \Delta x/2} \Big|_{\beta_j - \Delta y/2}^{\beta_j + \Delta y/2} \quad (4)$$

where $\alpha_i = \alpha_1 + i \cdot \Delta x$ and $\beta_j = \beta_1 + j \cdot \Delta y$ represent the central points of subdomain of piecewise integration.

Combining equations (3) and (4), the upward continuation integration (equation (1)) can be equivalently approximated by a matrix form (equation (5)),

$$\mathbf{U} = \mathbf{K} \mathbf{U}_0 \quad (5)$$

where $\mathbf{U} = [U_{11}, U_{21}, \dots, U_{m,n}]^T$ and $\mathbf{U}_0 = [U_{11}, U_{21}, \dots, U_{ij}]^T$ represent vector of discretized continued and observed field, respectively. \mathbf{K} is the

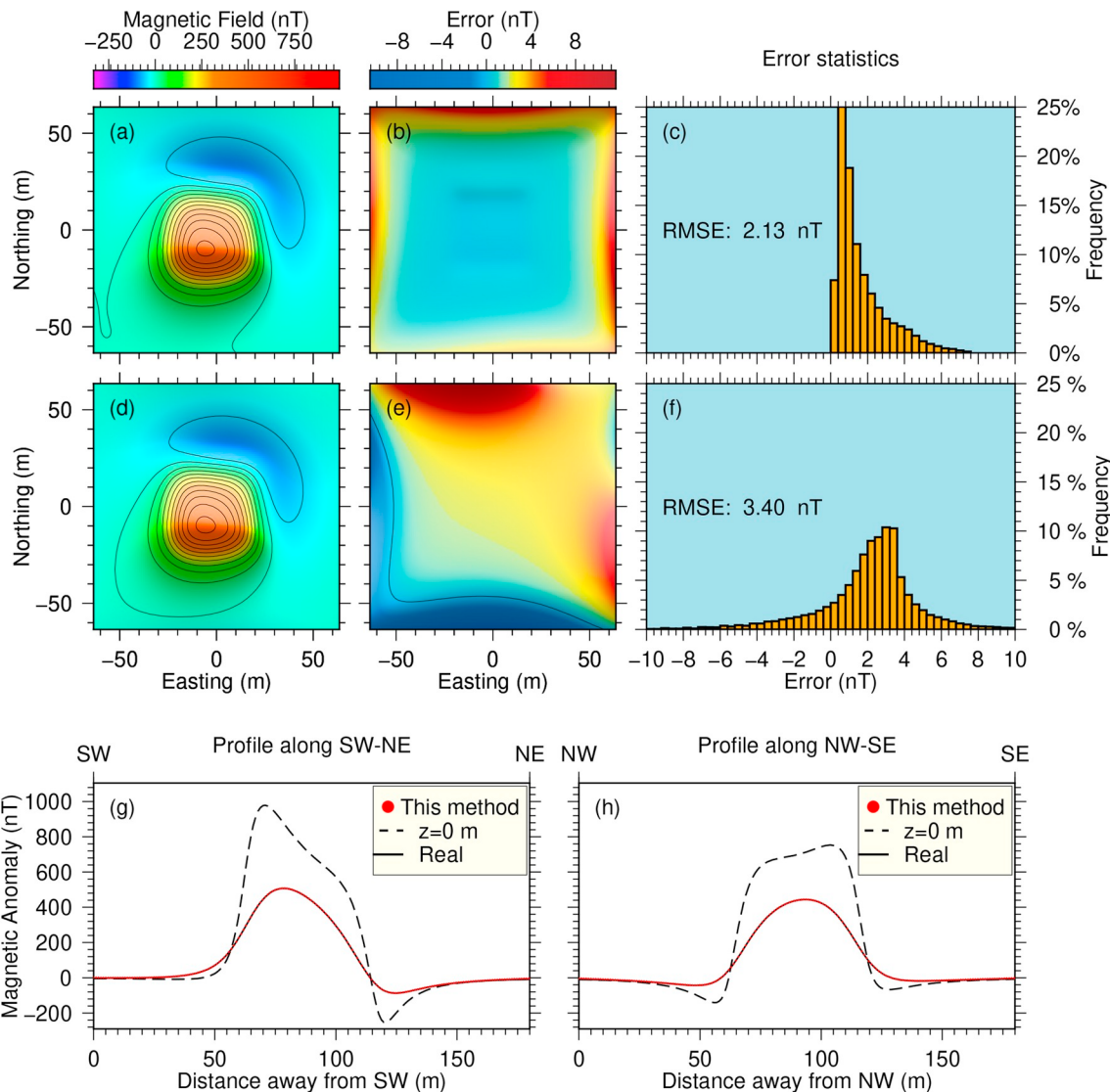


Fig. 5. Upward continuation of magnetic field (Fig. 4b) from plane of $z = 0$ to plane of $z = 8$ m. Which is calculated in the spatial domain (first row: a~c) and frequency domain (second row: d ~ f), respectively. (a) and (d) are upward continuation results. (b) and (e) are error distributions between the theoretical field (Fig. 4d) and continued field of (a) and (d), respectively. (c) and (f) are the error statistics of (b) and (e), respectively. Upward continuation calculated in the spatial domain gives smaller RMSE values. The accurate solution (black solid line), result of this method (red dot), and input data (dashed line) along the profile of SW-NE and NW-SE are shown in (g) and (h), respectively. (For interpretation of the references to color in this figure legend, the reader is referred to the Web version of this article.)

upward continuation kernel matrix with dimensions of $(M \times N, M \times N)$. The general form of the element can be written as equation (6),

$$k_{mn,ij} = \frac{1}{2\pi} P_{mn,ij} \quad (6)$$

Note that for the continuation from plane to plane, $\Delta z(x_m, y_n) = \Delta z$ is a constant; thus, the kernel matrix K is reduced to a blocked Toeplitz matrix whose elements can be derived from the first row. In this case, it will greatly reduce computing memory consumption. The transform formula can be expressed as equation (7),

$$k(m, n : i, j) = k(1, 1 : |i_0|, |j_0|) \cdot \text{sign}(i_0) \cdot \text{sign}(j_0), \quad \text{sign}(x) = \begin{cases} 1, & \text{if } x > 0 \\ 0, & \text{if } x = 0 \\ -1, & \text{if } x < 0 \end{cases} \quad (7)$$

2.2. Downward continuation

As an inverse problem of the upward continuation, downward

continuation can be solved from the first kind of Fredholm integral (equation (1)), which is expressed in matrix form (or linear equations) of equation (5). Solution of downward continuation is extremely sensitive to high-frequency perturbations of observed field data (right hand side of equation (5)). It means that linear equation (5) is a typical ill-posed problem (Hansen, 1994). Therefore, more sophisticated methods, for example regularization methods (e.g. Li et al., 2012; Zeng et al., 2013), or iterative methods (e.g. Hansen, 2002; Xu, 2006) must be applied to ensure that a meaningful solution is obtained. It must be noted that the kernel matrix K for downward continuation from surface to plane is no longer symmetric matrix; thus, this feature must be considered when using the conjugate gradient method.

2.3. Regularization and iteration

The instability of numerical solution of ill-posed problem (equation (5)), by its nature, arises from the cluster of small singular values of K . Therefore, it is necessary to compile further information of the desired

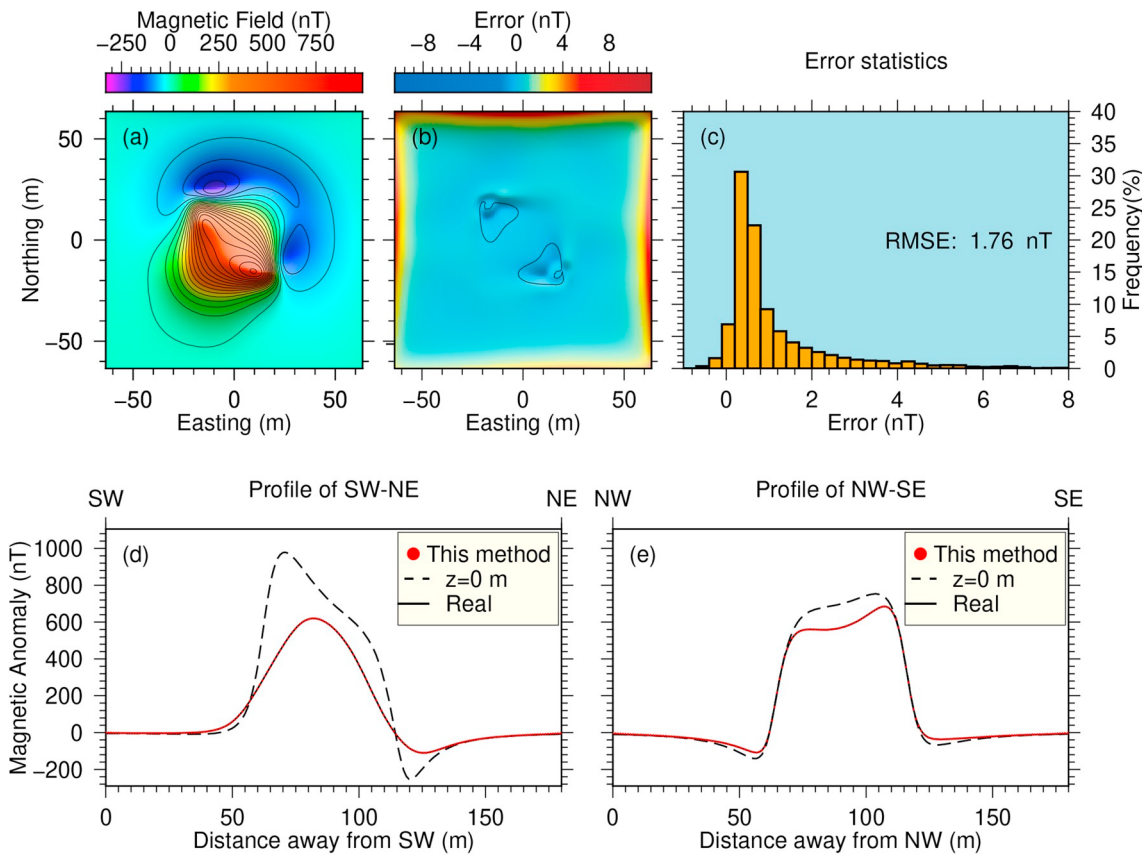


Fig. 6. Upward continuation of magnetic field (Fig. 4b) from plane of $z = 0$ m to surface (Fig. 4a). (a) Upward continuation result. (b) Error field between theoretical field (Fig. 4c) and continued field (a). (c) is the error statistics, the error of >70% calculation points is less than 1 nT and the points of larger error are located at the boundaries. The accurate solution (black solid line), result of this method (red dot), and input data (dashed line) along the profile of SW-NE and NW-SE are shown in (d) and (e), respectively. (For interpretation of the references to color in this figure legend, the reader is referred to the Web version of this article.)

solution to stabilize the problem and to obtain a stable solution with physically. This can be implemented by the regularization technique.

Comparing each method of solving linear equations for downward continuation is not the focus of this paper. Herein, we implement an iterative method which is simple but robust and similar to Landweber iteration (Hansen, 2002) and Integral-iteration methods (Xu, 2006). Let $\mathbf{U}^{(0)} = \mathbf{0}$ denote the starting solution guess; then, the iteration takes the form

$$\mathbf{U}^{(\tau)} = \mathbf{U}^{(\tau-1)} + \omega \mathbf{K}(\mathbf{U}_0 - \mathbf{K}\mathbf{U}^{(\tau-1)}) = \mathbf{U}^{(\tau-1)} + \omega \mathbf{K}\mathbf{R}^{(\tau-1)}, \quad \tau = 1, 2, 3, \dots \quad (8)$$

where $0 < \omega < 1$ is a real positive parameter whose value controls the behavior of the iterations. Because \mathbf{K} is a nonsymmetrical matrix, we utilize \mathbf{K} itself rather than \mathbf{K}^T to multiply residual $\mathbf{R}^{(\tau-1)}$. We can obtain a filter factor for this method, which is the same as the Landweber iteration, based on singular value decomposition (SVD) analysis (Hansen, 2002). The filter factors of these two iterative methods can be expressed as $f(\sigma) = 1 - (1 - \omega\sigma^n)^{\frac{1}{n}}$ which is shown in Fig. 3, where τ is the iteration number, σ is singular value, and ω is a coefficient. In particular, $n = 1$ and $n = 2$ represent Landweber iteration and Integral iteration, respectively. For downward continuation of noise-contaminated observed field data, Landweber iteration method suppresses tiny singular values well and is therefore more numerically stable.

3. Synthetic example

In order to examine the methods and algorithm, we simulated a set of synthetic models using regular grids for the topographic surfaces and magnetic field data. The observational field data are modelled on a plane

and a synthetic topographic surface expressed by Pilkington and Boulanger (2017),

$$z = f_0 \cdot \sin\left(\frac{4\pi xy}{x_m y_m}\right) e^{-\frac{|x^2+y^2|}{ax_m y_m}} \quad (9)$$

here $a = 0.2$, $f_0 = 10$, $x_m = \max(x)$, $y_m = \max(y)$, $x = [-63.5, 63.5]$ and $y = [-63.5, 63.5]$. In all the samples, the grid size is 128×128 . To compare with a previous study, a prism and topography model with the same parameters as Fig. 9 of Pilkington and Boulanger (2017) are employed to forward the synthetic magnetic field. The dimensions of the prism in meters are $x = [-20, 20]$, $y = [-20, 20]$, $z = [-20, -10]$, with a susceptibility of 0.1 SI, magnetic declination of 20° , and magnetic dip of 60° . The average magnetic intensity is assumed as 5×10^4 nT. The prism position, simulated topography, and theoretical magnetic field on different surfaces are shown in Fig. 4. The forward calculation is based on the open-source software Fatiando a Terra developed by Uieda et al. (2013). All the continuation methods are programmed in C++ and run on a desktop computer with a 2.7 GHz Intel Core i7 CPU. Table 1 shows the computation time and the number of iterations for synthetic examples. Two kinds of error formulae are used to measure the continued results quantitatively, the same form of root mean square error (RMSE) and relative error (RE) as equation (10),

$$RMSE = \sqrt{\frac{1}{n_x n_y} \sum_{i=1}^{n_x} \sum_{j=1}^{n_y} (U_{con} - U_{exact})^2}, \quad RE = \frac{\|U_{con} - U_{exact}\|_2}{\|U_{exact}\|_2}. \quad (10)$$

where U_{con} and U_{exact} represent continued results and theoretical magnetic field data, respectively.

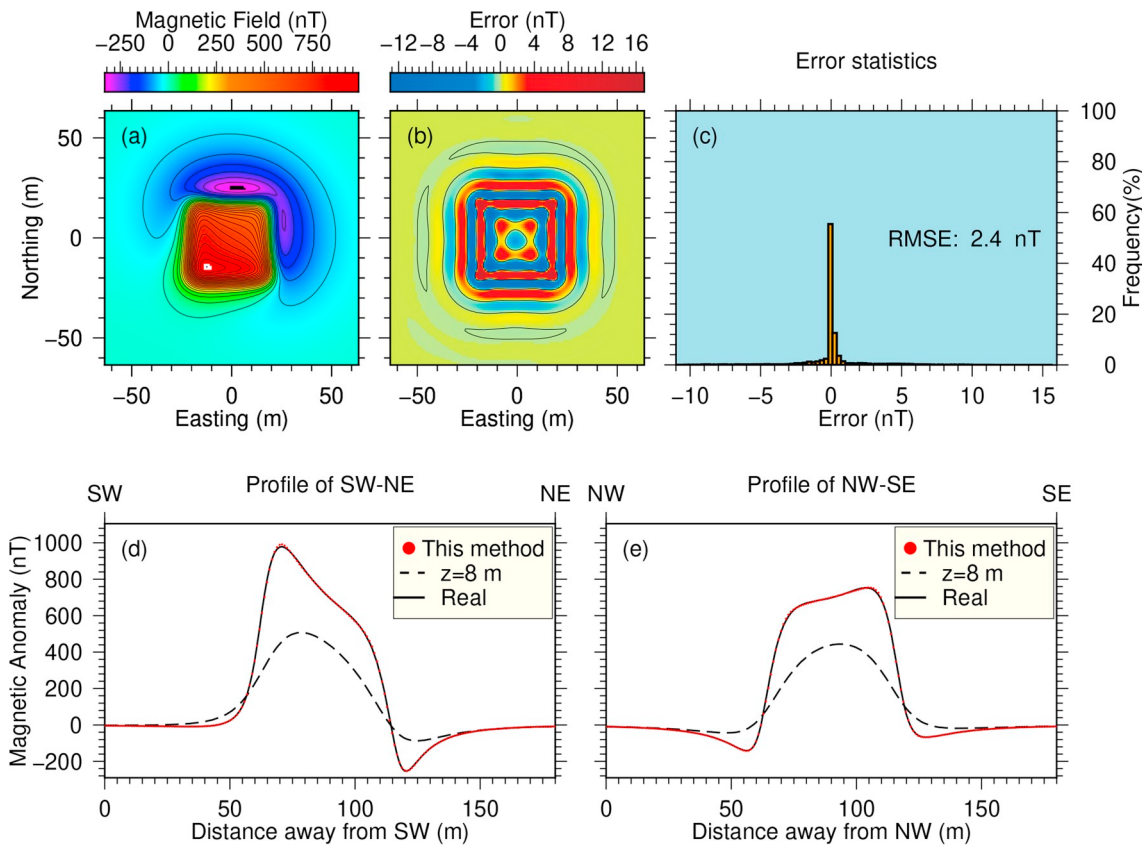


Fig. 7. Downward continuation of magnetic field (Fig. 4d) on level of $z = 8$ m to level of $z = 0$ m. This situation is corresponding to solve equation (8), in which U is known but U_0 is unknown, and kernel matrix is calculated by equation (6) with constant $\Delta z = 8$ m. (a) Downward continuation result. (b) Error distribution between theoretical field (Fig. 4b) and continued field (a). (c) shows the error statistics. The accurate solution (black solid line), result of this method (red dot), and input data (dashed line) along profile of SW-NE and NW-SE are shown in (d) and (e), respectively. (For interpretation of the references to color in this figure legend, the reader is referred to the Web version of this article.)

3.1. Upward continuation from level to level

This case is a forward problem of equation (5) that U_0 is known and kernel matrix K is calculated by equation (6) with constant Δz . We perform upward continuation of this synthetic magnetic field (Fig. 4b) from level $z = 0$ m to level $z = 8$ m using the new kernel function in the spatial domain. This upward continuation process is carried out by multiplying the kernel matrix by the observational field data vector (equation (5)) and can be easily implemented by parallel computation (e.g. OpenMP). For continuation from plane to plane, the kernel matrix (K) is a blocked symmetric matrix, the program only needs to store the first row and can therefore process large-data problems. The upward continuation results of these two methods are shown in Fig. 5. The error (Fig. 5b) of the space-domain method is basically distributed focus on boundaries, which is caused by insufficient data. From error statistics, more than 5% of the errors are in the range of 0–2 nT (Fig. 5c) for the space-domain method and 2–4 nT (Fig. 5f) for the FFT method. To visualize comparison between calculation result and accurate solution much more clear, data extracted along two profiles, SW-NE and NW-SE, are shown in Fig. 5 (g) and (h), respectively. The SW-NE profile is located along diagonal line from SW (southwest) corner to NE (northeast) corner, and the NW-SE profile is located along diagonal line from NW (northwest) corner to SE (southeast) corner.

3.2. Upward continuation from level to surface

In spatial domain, upward continuation from plane to surface is equivalent to calculate matrix product in equation (5), where U_0 is known and the kernel matrix K is calculated by equation (6), but Δz is

not a constant and given by input topography data of continued surface. Fig. 6 shows the results of upward continuation of the magnetic field (Fig. 4b) on the plane to a synthetic topography (Fig. 4a) based on the proposed space-domain method.

3.3. Downward continuation

Downward continuation as an inverse problem is based on upward continuation. To obtain a stable and reasonable numerical solution, we apply the iteration method (equation (8)) to solve the ill-posed linear equations (equation (5)). Downward continuation of the magnetic field from level to level and from surface to level are shown in Figs. 7 and 8, respectively. For downward continuation from surface to level, the continued field data is reconstructed from observed data (Fig. 4c) distorted by topography (Fig. 4a). It is similar to Fig. 6, where the continuation distance varies from 0 to 8 m as well. The computing time, RMSE, RE, and iteration number of these two kinds of downward continuation are shown in Table 1.

3.4. Numerical performance of downward continuation with noise-contaminated data

The Landweber iteration method is a classical method to solve ill-posed problem, and it suppresses noise by filtering tiny singular values, as shown in Fig. 3. To test the numerical performance of the Landweber iteration for downward continuation, we perform downward continuation of noise-contaminated field data and the results are shown in Fig. 9. Adding random noise with 0 nT mean and 1 nT standard deviation (SD) into noise-free magnetic field data (shown in Fig. 4c) as

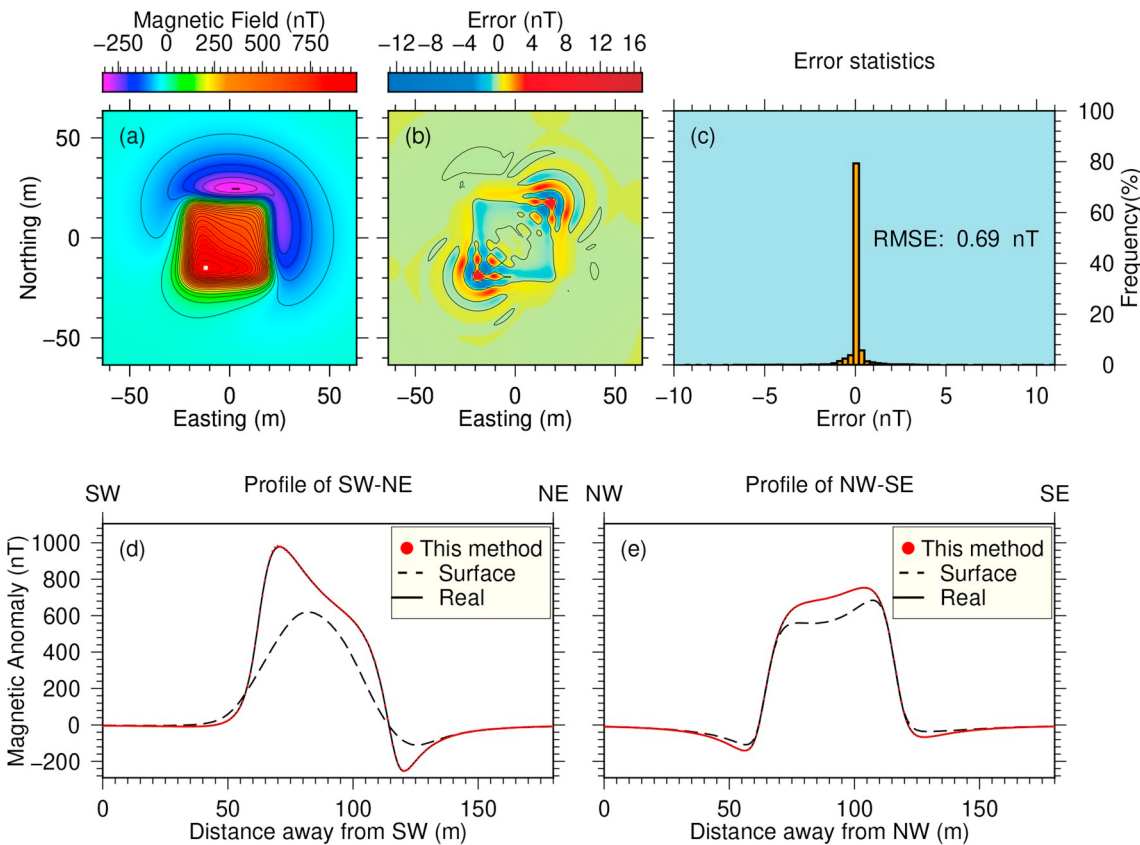


Fig. 8. Downward continuation of magnetic field (Fig. 4c) on surface (Fig. 4a) to level of $z = 0$ m. This situation is corresponding to solve equation (8), in which U is known and U_0 is unknown, kernel matrix is calculated by equation (6) and Δz is given by topography data of surface in Fig. 4a. (a) Downward continuation result. (b) Error distribution between theoretical field (Fig. 4b) and continued field (a). (c) shows the error statistics. The accurate solution (black solid line), result of this method (red dot), and input data (dashed line) along profile of SW-NE and NW-SE are shown in (d) and (e), respectively. (For interpretation of the references to color in this figure legend, the reader is referred to the Web version of this article.)

input noise-contaminated data. As shown in Fig. 3, the iteration number τ plays the role of the regularization parameter (Hansen, 2002): initially only the largest SVD components are included in the iteration solution $x^{(\tau)}$, and the smaller SVD components are included with increasing iteration number, and therefore amplifies the noise.

We propose a *fitting-smooth* curve (Fig. 10) to estimate iteration number. Using the l^2 -norm of the gradient $\text{grad}(U^{(\tau)})$ of the τ^{th} iterative continued field ($U^{(\tau)}$) as a proxy of *smooth* (equation (11)),

$$\|\text{grad}(U^{(\tau)})\|_2 = \sqrt{\sum_{i=1}^{M-1} \sum_{j=1}^{N-1} (U_x^{(\tau)} + U_y^{(\tau)})^2}, \quad U_x = \frac{U_{i+1,:}^{(\tau)} - U_{i,:}^{(\tau)}}{\Delta x}, \quad U_y = \frac{U_{:,j+1}^{(\tau)} - U_{:,j}^{(\tau)}}{\Delta x}, \quad (11)$$

where U_x and U_y represent derivative of the τ^{th} iterative continued field ($U^{(\tau)}$) in x and y direction, respectively. And using relative error of data fitting $R(U^{(\tau)})$ (see equation (8)) as a proxy of *fitting*. As iteration number increases, $R(U^{(\tau)})$ always decreases and $\text{grad}(U^{(\tau)})$ changes through three stages: increase-decrease-increase. For the first increase stage, the iteration is started from initial guess solution of observational field data (U_0) with a smaller gradient. As the iteration number increases, more and more detailed features will be added to the solution ($U^{(\tau)}$), and therefore increase its gradient. After the first stage, the error amplifying effect starts to increase and plays a major role after the second stage. The purpose of this method is to find an optimal iteration number, for fitting observation data and minimizing errors. The optimal iteration number corresponds to the minimum value in the decrease-increase stage of the curve. The variations of RMSE and fitting-smooth curve for downward continuation of noise-contaminated data (Fig. 9) are shown in Fig. 10 and $\tau = 277$ is the optimal iteration number.

4. Field data application

To examine the performance of the proposed numerical method when applied to real cases, we conducted an aeromagnetic survey of the Kluane area, the same area explored in the study by Pilkington and Boulanger (2017). The aeromagnetic and flight topography (or drape surface) data were taken from the Geological Survey of Canada data service (Coyle and Oneschuk, 2015), these data are shown in Fig. 11(a) and (b). The magnetic field values vary from -709 to 988 nT and the drape surface varies from 977 to 2190 m above sea level. The variation (>1200 m) in the drape surface is large but the mean terrain clearance (~ 116 m) is relatively small, the drape surface and the land surface are approximately parallel.

We first calculated the downward continuation of the aeromagnetic data from the drape surface to the base plane at 970 m, which is below the bottom of drape surface, to obtain a temporary field shown in Fig. 11c. The optimal iteration number $\tau = 441$ was determined from the *smooth-fitting* curve. Subsequently, the magnetic field on any surface above the base plane can be calculated by equation (5). Therefore, the continuation of potential field from observed surface to another surface could be achieved in a manner similar to that used by Pilkington and Thurston (2001). The upward continuation of the magnetic field from the flight surface to a horizontal plane at 2200 m is equivalent to upward continuation of the temporary field (Fig. 11c) to the same plane (2200 m). These results are shown in Fig. 11d, which corresponds to the last three rows of Fig. 11 in the report by Pilkington and Boulanger (2017). Fig. 11e shows the results of the upward continuation of the magnetic field from the flight surface to a parallel surface 200 m above. Fig. 11e corresponds to the last three rows of Fig. 13 in the paper by Pilkington

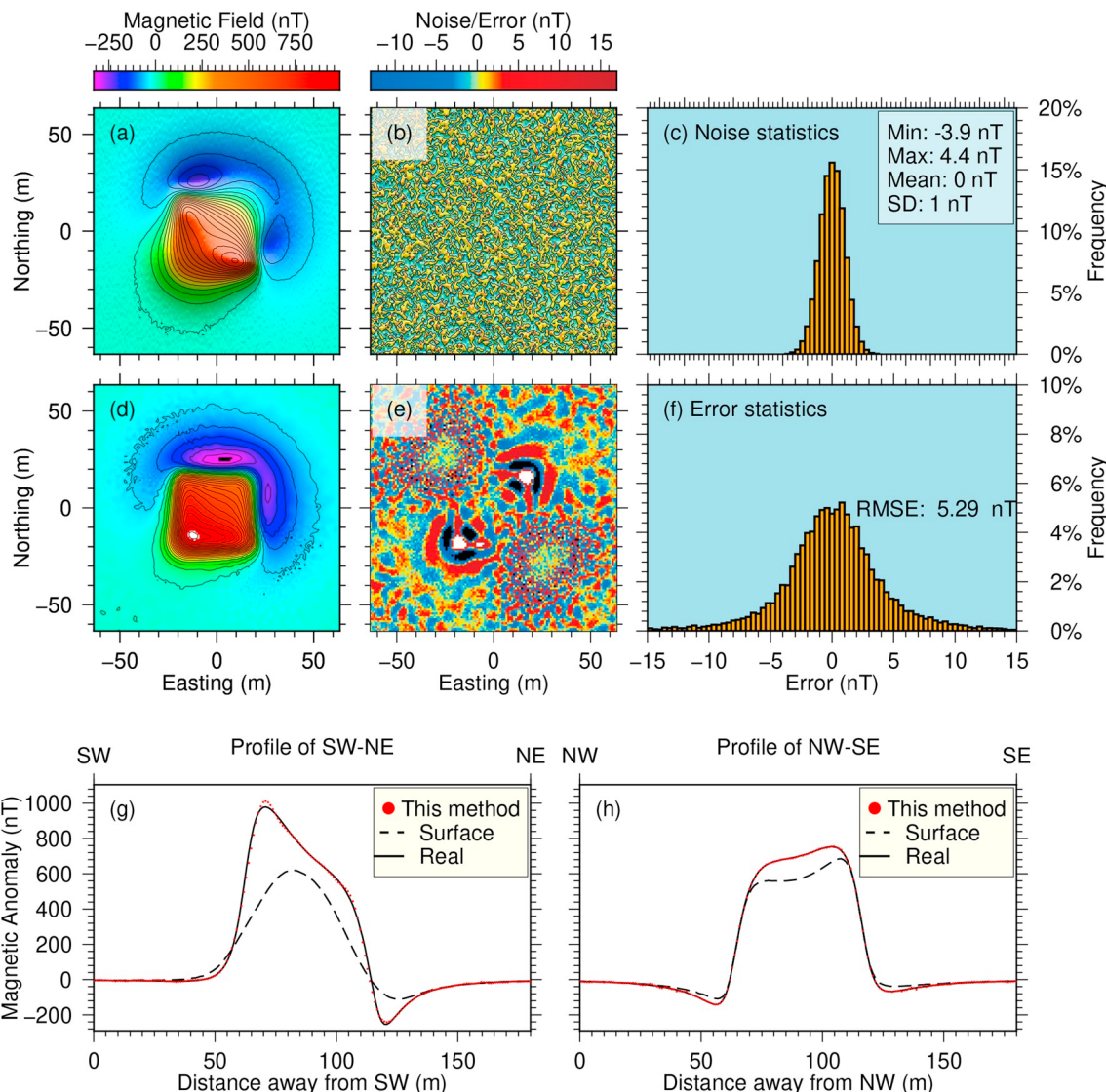


Fig. 9. Downward continuation of noise-contaminated magnetic field data from topography (shown in Fig. 4a) to plane $z = 0$ m. The noise-contaminated magnetic field data (a) is generated by adding noise (b) to noise-free magnetic field data, which is shown in Fig. 4c. (c) shows statistic histogram of noise data. The middle row shows the 277th iteration result (d), its difference field (e) with the exact solution (shown in Fig. 4b) and the statistic histogram (f) of downward continuation error distribution. The accurate solution (black solid line), result of this method (red dot), and input data (dashed line) along the profile of SW-NE and NW-SE are shown in (g) and (h), respectively. (For interpretation of the references to color in this figure legend, the reader is referred to the Web version of this article.)

and Boulanger (2017). The results shown in Fig. 11d and (e) have good consistency with the results obtained by Xia, Strakhov and Bhattacharya method which are reported by Pilkington and Boulanger (2017).

5. Discussion

Zhang et al. (2016) demonstrated a space-domain method of downward continuation, which could be regarded as a kind of spatial convolution method. The old kernel function (equation (23) in Zhang et al. (2016)) is obtained by directly taking the integral kernel out of the integral sign, which is rewritten as equation (12),

$$G(i, l, h) = \frac{1}{2\pi} \frac{h - h_0}{[(x(i) - x(l))^2 + (y(i) - y(l))^2 + (h - h_0)^2]^{3/2}} \quad (12)$$

It should be noted that there are large differences between the old and new kernel functions with the continuation distance Δz decreasing from 1 grid spacing to 0, which is indicated by the magenta curves in

gray region in Fig. 12. In addition, there is a singularity in equation (12) when $h = h_0$, $x(i) = x(l)$, and $y(i) = y(l)$, while the new kernel function is equal to one which corresponds to the case of $\Delta z = 0$ and the calculation point is (x_0, y_0) in Fig. 12.

To compare the numerical performance of the new and old kernel functions, we calculated the upward continuation of the magnetic field (shown in Fig. 4a) to the plane of 0.5 m (0.5 grid unit) using our code and the MATLAB code used by Zhang et al. (2016), which is available on Github (<https://github.com/zhangyle83/Geo-Data-Downward-Continuation>). The results are shown in Fig. 12. Except for the boundary effect, which is caused by limited data, the result calculated by the new method is accurate (RMSE = 0.73 nT, RE = 0.33%). In contrast, there is a large error in the amplitude of the result calculated via the code used by Zhang et al. (2016). For $\Delta z = 0$, the code used by Zhang et al. (2016) does not work. While the correct result calculated by the new method is equal with the input data because the new kernel matrix is an identity matrix.

The errors and singularity of the old kernel function is caused

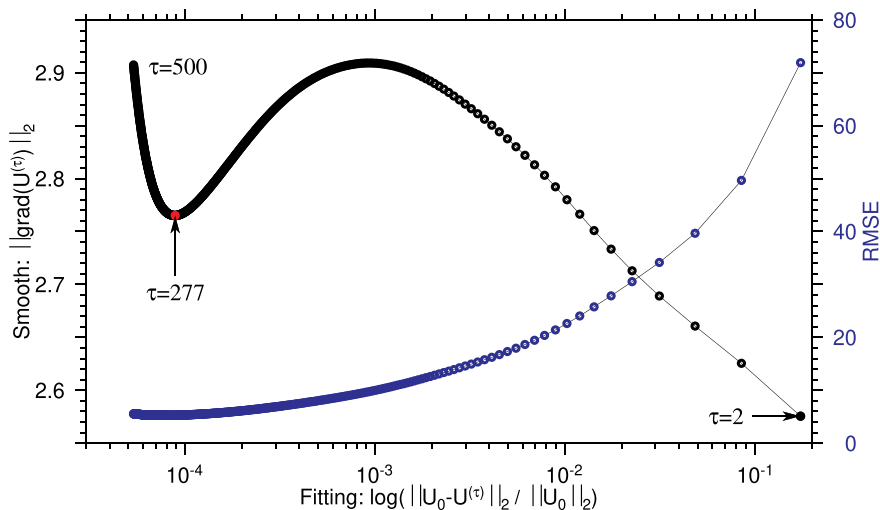


Fig. 10. The fitting-smooth curve for downward continuation of the noise-contaminated field data (shown in Fig. 9). The blue line is the REMS as a function of the data fitting error. τ is the iteration number and the red point is the optimal iteration number. (For interpretation of the references to color in this figure legend, the reader is referred to the Web version of this article.)

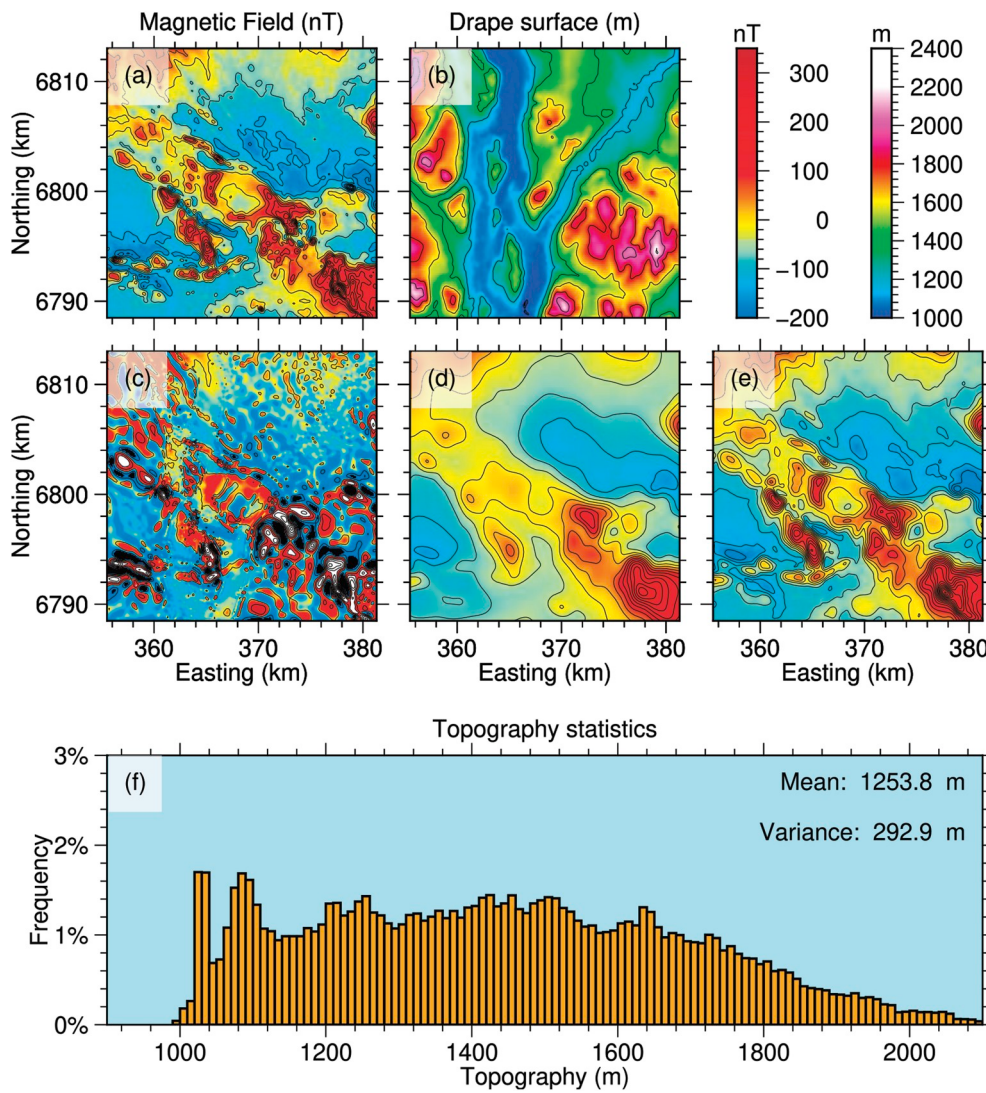


Fig. 11. Continuation of the real aeromagnetic data. All field plots are referenced with the same color bar. (a) Magnetic field anomaly observed on the flight (drape) surface, contour interval is 80 nT. (b) The flight (drape) surface, contour interval 200 m. (c) The equivalent field that is a downward continuation of the observed field to a horizontal plane, is at 970 m. (d) The magnetic field after upward continuation of the observed field from drape surface to a horizontal plane at 2200 m, contour interval, is 40 nT. (e) The magnetic field after upward continuation of the observed magnetic field to a parallel surface 200 m above the drape surface, contour interval, is 40 nT. (f) is the Statistic histogram of flight surface data (shown in b). (For interpretation of the references to color in this figure legend, the reader is referred to the Web version of this article.)

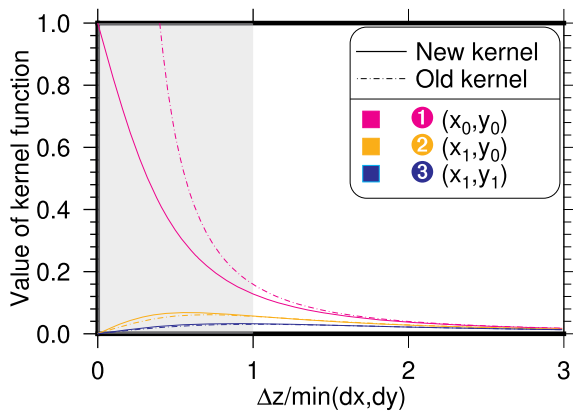


Fig. 12. The proposed new kernel function (equation (6)) and the old kernel function proposed by Zhang et al. (2016) changes with continuation distance (Δz), which is expressed as a multiple of the grid unit. The observational field point is set to (x_0, y_0) , which is shown as a red circle in Fig. 2; the horizontal position of three calculated points are also shown in Fig. 2 as colored i ($i = 1, 2, 3$). The solid curve and dash-dot curve in this figure represent the new and old kernel functions, respectively. The different colors correspond to different calculation points. (For interpretation of the references to color in this figure legend, the reader is referred to the Web version of this article.)

because $G(i, l, h)$, which is not a constant in the domain of integration (equation (2)), is directly taken outside of the integral. In contrast, the new kernel function (equation (4)) produces an exact solution by integration and does not produce a singularity or a large error for $\Delta z \geq 0$.

6. Conclusions

The analytical continuation of potential field data in the spatial

domain has several advantages over the frequency-domain method. The space-domain method is more accurate and more flexible when calculating the continuation between two surfaces, which are not always horizontal plane. Compared with a previous study, the method proposed in this paper has its theoretical completeness, which means the new kernel function is valid for all $\Delta z \geq 0$ and there is no singularity. The proposed method can be applied to calculate potential field data continuation from arbitrary observation surface to another surface. For downward continuation, the iteration method is robust for both noise-free and noise-contaminated data, and the optimal iteration number can be determined efficiently using the proposed smooth-fitting curve. We applied our proposed method to an aeromagnetic survey in the Kluane area and obtained acceptable results that show a good consistency with those obtained by Pilkington and Boulanger (2017).

Computer code availability

Name of code: conti2d.
 Developer: Zhikui Guo (zhikuiGuo@live.cn).
 Address: 36 Baohubeilu Rd. Hangzhou, 310012.
 Year first available: 2019.
 Hardware required: no specific requirement.
 Software required: fftw, netCDF, OpenMP, make, g++ or Microsoft Visual Studio 2017 for Windows system.
 Program language: C++
 Program size: 1.2 Mb.
Manual: https://github.com/zguoch/conti2d/blob/master/manual/manual_conti2d.pdf.
Tutorial video: <https://youtu.be/jQcnD3rnlgk>.
 Source code for Linux and Mac OS: <https://github.com/zguoch/conti2d>.
 Source code for Windows: <https://github.com/zguoch/conti2d/tree/win10/commandline/SourceCode>.

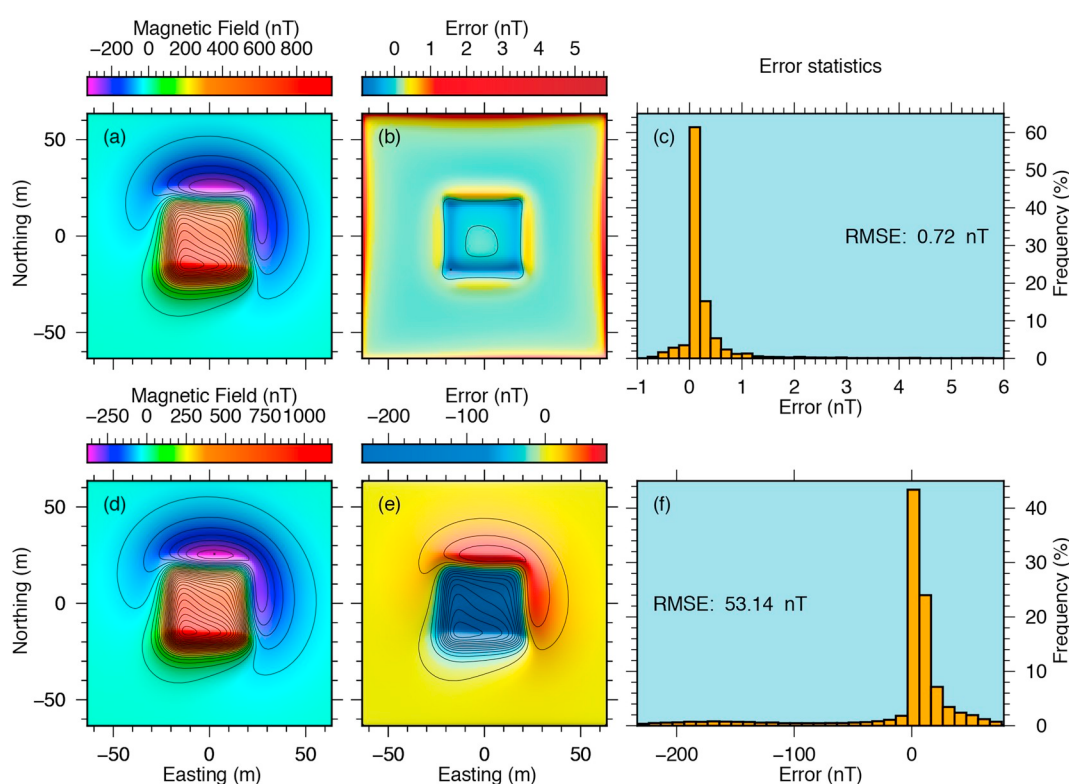


Fig. 13. Upward continuation of the magnetic field (shown in Fig. 4a) from plane $z = 0$ m to plane $z = 0.5$ m, calculated using the proposed new method (top row) and the method by Zhang et al. (2016) (bottom row). The first column shows the results of the upward continuation. The middle column shows the error (exact solution minus the first column). The last column shows the statistical histogram of the error distribution.

Executable file without GUI for Windows 7 and Windows 10 (x64) and example data: <https://github.com/zguoch/conti2d/tree/win10/commandline/PreCompiled>.

Executable file with GUI for Windows 7 and Windows 10 (x64) and example data: <https://github.com/zguoch/conti2d/tree/win10/GUI>.

Contribution of each author

Zhikui Guo derived equations, implemented the computer program and tested the algorithm using synthetic data and field data. Chunhui Tao proposed the original idea, improved text of the manuscript and provide funding for this study.

Declaration of competing interest

There is no conflict of interest.

Acknowledgments

We thank Dr. Du and Dr. Liang for their suggestions. This study was promoted by the National Key R&D Program of China (2018YFC0309901 and 2017YFC0306203) COMRA Major Project, China under contract No. DY135-S1-01-01 and No.DY135-S1-01-06. It was also supported by the China Scholarship Council (NO. 201706410085).

Appendix A. Supplementary data

Supplementary data to this article can be found online at <https://doi.org/10.1016/j.cageo.2020.104405>.

References

- Abtahi, S.M., Pedersen, L.B., Kamm, J., Kalscheuer, T., 2016. Consistency investigation, vertical gravity estimation, and inversion of airborne gravity gradient data — a case study from northern Sweden. *Geophysics* 81, B65–B76.
- Baranov, W., 1975. Potential fields and their transformations in applied geophysics. *Geoexplor. Monogr.* 6, 121.
- Blakely, R.J., 1996. Potential Theory in Gravity and Magnetic Applications. Cambridge University Press.
- Caratori, T.F., Ronde, C., Yoerger, D., Kinsey, J., Tivey, M., 2012. 3-D focused inversion of near-seafloor magnetic data with application to the Brothers volcano hydrothermal system, Southern Pacific Ocean, New Zealand. *J. Geophys. Res.: Solid Earth* 117.
- Cooper, G., 2004. The stable downward continuation of potential field data. *Explor. Geophys.* 35, 260–265.
- Coyle, M., Oneschuk, D., 2015. Residual Total Magnetic Field, Kluane Lake West Aeromagnetic Survey, Yukon, NTS 115-G/12 and Parts of 115-G/11, 13, 14 and 115-F/9, 16. Geological Survey of Canada. Open File 7912, 1 sheet.
- Fedi, M., Florio, G., 2002. A stable downward continuation by using the ISVD method. *Geophys. J. Int.* 151, 146–156.
- Fedi, M., Paoletti, V., Rapolla, A., 2005. The role of multilevel data in potential field interpretation. *Comput. Geosci.* 31, 681–688.
- Geuzaine, C., Jean François, R., 2009. Gmsh: a 3-D finite element mesh generator with built-in pre-and post-processing facilities. *Int. J. Numer. Methods Eng.* 79, 1309–1331.
- Gonçalves, I.G., Kumaira, S., Guadagnini, F., 2017. A machine learning approach to the potential-field method for implicit modeling of geological structures. *Comput. Geosci.* 103, 173–182.
- Gross, L., Altinay, C., Shaw, S., 2015. Inversion of potential field data using the finite element method on parallel computers. *Comput. Geosci.* 84, 61–71.
- Guspí, F., 1987. Frequency-domain reduction of potential field measurements to a horizontal plane. *Geoexploration* 24, 87–98.
- Hansen, P.C., 1994. Regularization tools: a Matlab package for analysis and solution of discrete ill-posed problems. *Numer. Algorithms* 6, 1–35.
- Hansen, P., 2002. Deconvolution and regularization with Toeplitz matrices. *Numer. Algorithms* 29, 323–378.
- Ivan, M., 1986. On the upward continuation of potential-field data between irregular surfaces. *Geophys. Prospect.* 34, 735–742.
- Li, Y., Devriese, S.G.R., Krahenbuhl, R.A., Davis, K., 2012. Enhancement of magnetic data by stable downward continuation for UXO application. *IEEE Trans. Geosci. Remote Sens.* 51, 3605–3614.
- Liu, S., Hu, X., Xi, Y., Liu, T., 2015. 2D inverse modeling for potential fields on rugged observation surface using constrained Delaunay triangulation. *Comput. Geosci.* 76, 18–30.
- Ma, G., Li, L., 2012. Edge detection in potential fields with the normalized total horizontal derivative. *Comput. Geosci.* 41, 83–87.
- Mauri, G., Williams-Jones, G., Ginette, S., 2011. MWTrmat—application of multiscale wavelet tomography on potential fields. *Comput. Geosci.* 37, 1825–1835.
- Oliveira, S.P., Ferreira, F., Souza, J., 2017. Edge Detect PFI: an algorithm for automatic edge detection in potential field anomaly images-application to dike-like magnetic structures. *Comput. Geosci.* 103, 80–91.
- Pašteka, R., Karcol, R., Kušnírák, D., Mojzeš, A., 2012. Regcont: a Matlab based program for stable downward continuation of geophysical potential fields using Tikhonov regularization. *Comput. Geosci.* 49, 278–289.
- Pilkington, M., Boulanger, O., 2017. Potential field continuation between arbitrary surfaces — comparing methods. *Geophysics* 82, J9–J25.
- Pilkington, M., Thurston, J.B., 2001. Draping corrections for aeromagnetic data: line-versus grid-based approaches. *Explor. Geophys.* 32, 95.
- Strakhov, A.V., Devtysyn, V.N., 1965. The reduction of observed values of a potential field to values at a constant level. *Phys. Solid Earth* 4, 256–261.
- Trompat, H., Boschetti, F., Hornby, P., 2003. Improved downward continuation of potential field data. *Explor. Geophys.* 34, 249–256.
- Uieda, L., Oliveira Jr., V.C., Barbosa, V.C.F., 2013. Modeling the Earth with Fatiando a Terra. Proceedings of the 12th Python in Science Conference, pp. 91–98.
- Wang, J., Meng, X., Fang, L., 2015. A computationally efficient scheme for the inversion of large scale potential field data: application to synthetic and real data. *Comput. Geosci.* 85, 102–111.
- Xu, S.Z., 2006. The integral-iteration method for continuation of potential fields. *Chin. J. Geophys.* 49, 1054–1060.
- Xu, S.Z., Yang, C.H., Dai, S., Zhang, D., 2003. A new method for continuation of 3D potential fields to a horizontal plane. *Geophysics* 68, 1917–1921.
- Yañez, G., Hernan, U., Jaime, A.V., 2018. Topographic correction of magnetic data on rugged topography with application to Río Blanco-Los Bronces and El Teniente porphyry copper districts, Southern Andes, Chile. *Explor. Geophys.* 49, 595–607.
- Zeng, X., Li, X., Su, J., Liu, D., Zou, H., 2013. An adaptive iterative method for downward continuation of potential field data from a horizontal plane. *Geophysics* 78, J43–J52.
- Zhang, Y., Wong, Y.S., Lin, Y., 2016. BTTB-RRCG method for downward continuation of potential field data. *J. Appl. Geophys.* 126, 74–86.